

A Three-State Thermodynamically Consistent Cross-Bridge Model for Muscle Contraction

Yiwei Wang^{1,*} and Chun Liu²

¹Department of Mathematics, University of California, Riverside, Riverside, CA, 92521, United States

²Department of Applied Mathematics, Illinois Institute of Technology, Chicago, IL, 60616, United States

*Correspondence: yiweiw@ucr.edu

ABSTRACT Muscle contraction is a prototypical multiscale chemomechanical process in which ATP hydrolysis at the molecular level drives force generation and mechanical work at larger scales. A long-standing challenge is to connect microscopic cross-bridge dynamics to macroscopic observables while retaining an explicit, thermodynamically consistent energetic budget for chemical-to-mechanical transduction. Here we use the Energetic Variational Approach (EnVarA) to unify Hill's cycle-affinity viewpoint with Huxley's sliding-filament mechanics within a single thermodynamically closed framework. We formulate a three-state Fokker–Planck–jump description for cross-bridge populations evolving on state-dependent free-energy landscapes, in which ATP hydrolysis enters through local detailed balance and biases the transition rates. Filament sliding velocity is incorporated as a convective transport mechanism in the Fokker–Planck dynamics, so that mechanical power exchange with the external motion emerges transparently from the resulting energy-dissipation law together with chemical input and irreversible dissipation. Under chemostatted conditions and a fast-equilibration closure for the attached substates, the model reduces to a closed two-state molecular motor description; in a further singular limit, this reduction recovers a Huxley-type transport–reaction equation. Proof-of-concept simulations of the reduced model reproduce a Hill-like force–velocity relation and show how ATP availability modulates the force–velocity curve while preserving its characteristic Hill-type shape.

SIGNIFICANCE We present a thermodynamically consistent, variational model that combines a three-state chemo-mechanical cycle with Fokker–Planck type equations on state-dependent energy landscapes within the energetic variational approach. In this formulation, macroscopic filament sliding enters directly as a transport term in the Fokker–Planck equations, and the mechanical work delivered to the external sliding is derived from the energy-dissipation law. The resulting closed energy-dissipation balance serves as a bookkeeping principle that cleanly partitions chemical input, mechanical power exchange, and irreversible dissipation. Under chemostatted conditions and a fast-equilibration closure for the attached substates, we derive a reduced two-state molecular motor model; in an additional singular limit, this reduction recovers a Huxley-type transport–reaction equation. We include proof-of-concept simulations of the reduced model showing Hill-like force–velocity behavior and illustrating how varying ATP availability can reshape the predicted force–velocity relation.

INTRODUCTION

Muscle contraction is a prototypical *multiscale* chemomechanical system that underlies animal locomotion and cardiovascular function. Muscle can be considered as an active viscoelastic material (1, 2). Its function emerges from a complex multiscale chemo-mechanical interaction: ATP hydrolysis and conformational changes of myosin at the nanometer scale generate force and motion at the level of individual cross-bridges (3); these microscopic events synchronize within the ordered architecture of sarcomeres and myofibrils (micrometers), and ultimately give rise to macroscopic mechanical responses of fibers, tissues, and whole organs. Moreover,

muscle, particularly *striated* muscle, is one of the few active biological materials for which *multiscale data* are available in a comparatively systematic manner. Structural and dynamical information spanning near-atomic resolution to sarcomere-level organization can be probed by X-ray diffraction and related techniques (4), while mesoscopic and macroscopic mechanical behavior is routinely quantified through assays such as laser diffractometry and force–velocity measurements (5). This unique combination of a strongly multiscale mechanism and richly multiscale measurements makes muscle an ideal testbed for developing predictive, thermodynamically consistent models that *bridge* molecular energy transduction

and emergent constitutive behavior.

There is a long history of developing mathematical models for muscle contraction. At the macroscopic scale, the active behavior of muscle can be described by a simple but remarkable force–velocity relation

$$V = b \frac{F_0 - F}{F + a} \quad (1)$$

proposed by A.V. Hill in 1938 (6). Here, V is the constant shortening velocity of muscle, F is the constant force, a , b and F_0 are model parameters. One can note that $V_{\max} = \frac{bF_0}{a}$, which is the velocity at which muscle shortens when there is no load. In the meantime, $V = 0$ when $F = F_0$. Hence F_0 is called the isometric or stall force. One can rewrite Eq. 1 as

$$b(F_0 - F) = FV + aV, \quad (2)$$

which formally corresponds to the first law of thermodynamics $dU = dW + dQ$, where aV is the heat and FV is the work. The two parameters, a and b , are the frictional heat generated by unloaded muscle shortening and the product of the muscle ATPase rate and the myosin step size (7).

To explain the physiological origin of Hill's equation, at the mesoscopic/microscopic scale, A.F. Huxley proposed a simple two-state model to describe the myosin–actin interaction (8), based on the sliding-filament hypothesis (9, 10). In Huxley's model, the myosin heads are modeled as spring-like elements that can attach to and detach from actin with displacement-dependent rates; the distribution of attached cross-bridges evolves under filament sliding and reaction kinetics. Let x denote the relative displacement of an actin binding site with respect to the myosin head, and assume that, at any instant, each head can interact with at most one nearby binding site. A detached head attaches to the actin site at relative displacement x with a rate, $f(x)$. Conversely, due to the free-energy releasing process (ATP hydrolysis), the myosin head can detach from actin with a rate $g(x)$. With $n(x, t)$ being the fraction of attached cross-bridges, the dynamics is described by

$$\frac{\partial n}{\partial t} - V \frac{dn(x)}{dx} = (1 - n(x))f(x) - g(x)n(x), \quad (3)$$

where $V > 0$ is the shortening (contracting) velocity. Here, we follow Huxley's original sign convention that shortening velocity carries cross-bridges with a certain displacement into smaller values of displacement (11). The macroscopic force follows from averaging the force per attached bridge over the attached population, $F(x) = pn(x)$, where p is the force produced per attached bridge, and $n(x)$ is the steady state of Eq. 3. With suitable assumptions of $f(x)$, $g(x)$ and p , Huxley-type models can reproduce force–velocity measurements (12).

The Huxley model has been the foundation for a vast amount of subsequent work (12–32) and is still useful for many purposes. These models can be classified into chemistry-based and mechanics-based models (31, 33). The first is a *chemistry-based* approach, which refines the original two-state scheme by introducing additional biochemical states and

strain-dependent transition rates, with the classical four-state Lymn–Taylor cycle as a prominent example (15). The second is a *mechanics-based* approach, which resolves the myosin head dynamics as stochastic motion on state-dependent free-energy landscapes, often cast in the language of Brownian ratchets (29, 34, 35). Although these viewpoints appear different, they can be interpreted as different resolutions of a common underlying picture: landscape-based stochastic dynamics at the continuous level (e.g., Klein–Kramers or Fokker–Planck descriptions) can be coarse-grained, under suitable time-scale separation, into discrete-state master equations that describe transitions among metastable states.

Starting in the early 1970s, T.L. Hill and collaborators made fundamental contributions toward placing such kinetic descriptions on a thermodynamically consistent picture (36–39). Rather than proposing a competing mesoscale equation, their work emphasized how chemical driving from ATP hydrolysis constrains transition kinetics through free-energy differences and cycle affinities, and how mechanical forces and work can be computed from the underlying energetic landscape. This energetic viewpoint provides a general link between chemical potential differences and mechanical performance and has profoundly influenced subsequent theories of molecular motors (24, 35, 40–49). Although we focus on actin–myosin, similar thermodynamic principles apply broadly across motor families, including microtubule-based kinesin and dynein (3, 50–53).

Despite their empirical success, most Huxley-type models are thermodynamically incomplete: the transition rates are typically fitted phenomenologically and lack explicit dependence on the chemical-potential difference associated with ATP hydrolysis (11, 54). Consequently, they cannot quantitatively predict the energy conversion efficiency or the thermal response of contracting muscle (55, 56). In contrast, the nonequilibrium thermodynamic formulation developed by Terrell L. Hill and collaborators (36, 38, 39), where reaction fluxes and mechanical forces are driven by free-energy differences, provides a rigorous energetic foundation for chemomechanical cross-bridge cycling, but does not by itself specify a spatially resolved overdamped stochastic dynamics for the strain coordinate, e.g., a Smoluchowski/Fokker–Planck equation coupled to filament sliding, needed to connect molecular cycling to Huxley-type transport–reaction descriptions and macroscopic force–velocity behavior (57).

Another emerging issue is how to build predictive models that can span scales from the dynamics of a single myosin molecule to the sarcomere scale, which contains millions of myosin molecules. At the microscopic scale, molecular dynamics models now provide deep insight into the functional dynamics of single myosin molecules, including interactions with various nucleotides (30). However, such modeling approaches are computationally intensive and cannot be scaled to the millions of interacting molecules that constitute a single sarcomere. Conversely, the majority of existing macroscopic models are phenomenological and couple the different

subsystems sequentially rather than treat them properly as simultaneous, coupled processes. As such, although these models can well fit a given set of experimental data, they provide limited insight into microscopic mechanisms and have limited predictive power (31) with their reliance on empirical parameters that may or may not have physical meaning. More importantly, a quantitative and thermodynamically consistent framework that links molecular energy transduction to emergent force–velocity behavior across scales is still missing.

In this work, we present an expository and computational study that uses the energetic variational approach (EnVarA) to formulate a minimal, thermodynamically consistent three-state cross-bridge model at the single-head scale. We develop a strain-resolved Fokker–Planck–jump framework in which cross-bridge populations evolve on state-dependent free-energy landscapes and undergo chemomechanical transitions constrained by local detailed balance.

A central conceptual point is how to maintain a consistent energetic budget in the presence of chemical driving. In many chemostatted motor or cross-bridge models, a closed energy-dissipation law is difficult to obtain because the nucleotide chemical potentials are prescribed; as a result, nonequilibrium driving is often represented in an ad hoc manner by *tilting* mechanical energy landscapes using $\Delta\mu$. Here we avoid such constructions by embedding Hill’s three-state cycle directly into an energy-dissipation framework: the chemical affinity enters through local detailed balance, biasing reaction propensities rather than altering the potential energy surface. More precisely, we treat ATP, ADP, and inorganic phosphate as reacting and diffusing chemical species, meaning chemical potentials become spatiotemporal variables rather than fixed parameters. This feature allows the chemical driving to emerge dynamically, enabling the study of ATP-limited regimes, supply-demand imbalances, and fatigue-like conditions. This yields a thermodynamically closed description and provides a clearer interpretation of how $\Delta\mu$ is transmitted to force generation and effective attachment/detachment kinetics. As a result, the formulation enables definitions of macroscopic force, mechanical power output, and energetic efficiency in the level of energy-dissipation law.

To connect with classical reduced descriptions, we consider a chemostatted regime and a fast-equilibration limit between attached substates, under which we derive an effective two-state Fokker–Planck-type model for molecular motors and a Huxley-type sliding-filament model, clarifying how chemical driving reshapes the effective energy landscape and alters attachment and detachment rates.

Finally, we provide proof-of-concept numerical experiments within this focused regime. We compute steady states of the reduced two-state model and obtain its force–velocity relation, showing that it reproduces a Hill-type force–velocity curve. By varying the chemostatted ATP level, we further demonstrate how nucleotide availability systematically modulates the force–velocity relation while preserving its characteristic Hill-like shape.

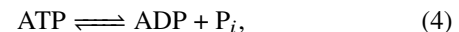
MATHEMATICAL MODEL

T.L. Hill’s cycle thermodynamics on state-dependent energy landscapes

We begin with T. L. Hill’s nonequilibrium-thermodynamic viewpoint for cross-bridge cycling (58). In Hill’s formulation, mechanical force and chemical kinetics are constrained by a common energetic structure. This framework is fundamentally a kinetic description on a discrete state space, and it does not rely on a variational principle or partial differential equations. Likewise, Duke’s molecular model provides a concrete, computable parametrization of the state-dependent free-energy landscapes, but it is not posed as a variational or PDE-based theory. These classical constructions nevertheless provide the key physical ingredients that we will later embed into an EnVarA-derived continuum description.

Let x denote an effective strain-like coordinate describing the relative displacement between a myosin head and its actin binding site. For state i , let $G_i(x)$ be the Gibbs free energy along this coordinate. For mechanically attached states, the force acting on the myosin head due to the potential $G_i(x)$ is $-\partial_x G_i(x)$. Since the muscle tension is defined as the force exerted by the head against the filament load, it carries the opposite sign. Therefore, we define the cross-bridge force generated by each head at state i as $F_i(x) = \partial_x G_i(x)$.

ATP hydrolysis provides the nonequilibrium driving,



and we represent chemical forcing by the chemical potential difference

$$\Delta\mu = \mu_{\text{ATP}} - \mu_{\text{ADP}} - \mu_{\text{P}_i}. \quad (5)$$

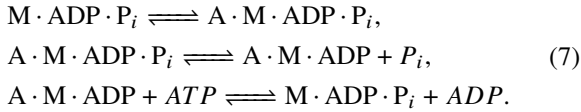
In the chemostatted setting, $\Delta\mu$ is treated as a prescribed parameter controlling how far the system is driven from equilibrium.

A two-state attachment–detachment description, involving only unattached and attached states, can reproduce basic force–velocity relations phenomenologically. However, such a model might be thermodynamically incomplete. In a two-state Markov description, $\Delta\mu$ may bias the attachment–detachment rate ratio and thus alter the steady-state occupancy and mean force; however, the lack of a closed chemomechanical loop makes it impossible to assign $\Delta\mu$ as a genuine cycle affinity with step-resolved energetic bookkeeping. In a strictly two-state Markov system, the chemical potential difference $\Delta\mu$ cannot enter as a genuine cycle-driving affinity, because no closed chemical–mechanical loop exists. As a result, the steady-state probability flux must vanish, precluding continuous ATP consumption and sustained mechanical power output. This structural limitation necessitates the introduction of at least a third state in order to form a minimal nonequilibrium chemomechanical cycle. Hill therefore introduced a

three-state cross-bridge cycle consisting of

- State 1: $M \cdot ADP \cdot P_i$ (detached),
- State 2: $A \cdot M \cdot ADP \cdot P_i$ (attached, pre-stroke), (6)
- State 3: $A \cdot M \cdot ADP$ (attached, post-stroke).

To represent sustained ATP consumption and mechanical power, the state network must contain a closed chemomechanical cycle:



Let $\alpha_{ij}(x)$ denote the transition rate $i \rightarrow j$ at position x . Thermodynamic consistency is enforced by local detailed balance,

$$\frac{\alpha_{ij}(x)}{\alpha_{ji}(x)} = \exp(-\beta [G_j(x) - G_i(x) - \Delta\mu_{ij}]), \quad \beta = (k_B T)^{-1}, \quad (8)$$

where $\Delta\mu_{ij}$ accounts for chemical potentials associated with the elementary step; in particular, $\Delta\mu_{12} = 0$, $\Delta\mu_{23} = \mu_{P_i}$, and $\Delta\mu_{31} = \mu_{ATP} - \mu_{ADP}$. Summing the logarithmic ratios around the directed cycle yields the total affinity $\beta\Delta\mu$, and we have

$$\sum_{\text{cycle}} \log \frac{\alpha_{ij}}{\alpha_{ji}} = \frac{\Delta\mu}{k_B T}, \quad (9)$$

Equation Eq. 9 characterizes the fundamental non-equilibrium nature of the system (33). In a physiological context, the cell's metabolic machinery maintains ATP, ADP, and P_i at concentrations far from their equilibrium ratios (33). This cycle affinity acts as a non-conservative "chemical battery" that breaks detailed balance, sustaining a persistent circulation (a non-zero net flux) through the state network. This driving force prevents the system from relaxing to thermal equilibrium, instead supporting a non-equilibrium steady state (NESS). Conversely, the equilibrium limit $\Delta\mu = 0$ restores detailed balance, forcing the steady-state cycle flux to vanish and halting the directed mechanical output (33).

The thermodynamic affinity $\Delta\mu$ provides the necessary "fuel" for the motor, but the actual transduction of chemical energy into directed mechanical work is governed by the spatial profiles of the free-energy landscapes. In (23), Duke proposed explicit forms of the free-energy landscapes based on an elastic element and a power-stroke shift.

$$\begin{aligned} G_1(x) &= 0, \quad G_2(x) = -\Delta G_{\text{bind}} + \frac{\kappa}{2} x^2, \\ G_3(x) &= -\Delta G_{\text{bind}} - \Delta G_{\text{stroke}} + \frac{\kappa}{2} (x + d)^2, \end{aligned} \quad (10)$$

where κ is an effective stiffness, d is the stroke distance, and ΔG_{bind} and ΔG_{stroke} encode binding and power-stroke energy changes.

Although Hill's theory established the energetic foundation for chemo-mechanical coupling, most implementations remain kinetic rather than variational: the free-energy and dissipation functions are not formulated as conjugate pairs within a unified energetic framework. Moreover, thermal noise and hydrodynamic coupling are usually introduced phenomenologically. To ensure energetic closure and directly link microscopic stochastic dynamics to macroscopic constitutive behavior, we next reformulate the cross-bridge model within the *Energetic Variational Approach* (EnVarA), leading to a Fokker-Planck-type description consistent with Hill's thermodynamic principles.

Energetic variational approach (EnVarA)

We briefly introduce EnVarA, a general framework for building thermodynamically consistent variational models of a complex system through its energy and rate of energy dissipation (59, 60). Like other variational principles, such as Onsager's variational principle (61–63) and the general equation for the non-equilibrium reversible-irreversible coupling (GENERIC) (64, 65), EnVarA is rooted in nonequilibrium thermodynamics, especially the seminal work of Rayleigh (66) and (67, 68). The key idea is that all dynamics, including those in biology, must be compatible with the first and second laws of thermodynamics. The first law expresses energy conservation as

$$\frac{d}{dt}(\mathcal{K} + \mathcal{U}) = \delta W + \delta Q, \quad (11)$$

where \mathcal{K} and \mathcal{U} denote the kinetic and internal energy, respectively, and δW , δQ represent the rate of mechanical work and heat input. These quantities are path-dependent and are not exact differentials. The second law quantifies irreversibility via

$$TdS = \delta Q + \Delta, \quad (12)$$

where T is the absolute temperature, S is the entropy, and $\Delta \geq 0$ denotes the rate of entropy production. For an isothermal and mechanically isolated system (i.e., $\delta W = 0$ and T constant), subtracting Eq. 12 from Eq. 11 yields the energy-dissipation law (69)

$$\frac{d}{dt}E^{\text{total}} = -\Delta(t) \quad (13)$$

where E^{total} is the total energy, including both the kinetic energy \mathcal{K} and the Helmholtz free energy $\mathcal{F} = \mathcal{U} - TS$, and $\Delta(t) \geq 0$ is the rate of energy dissipation, which is equal to the entropy production in the isothermal case. We do not discuss the non-isothermal case in the current work, and refer to (70) and (60) for detailed treatments under EnVarA. The goal of modeling is to determine the exact forms of the energy and dissipation functionals.

Starting from an energy-dissipation law (Eq. 13), EnVarA derives the governing dynamics by combining the least action principle (LAP) for conservative effects with the maximum

dissipation principle (MDP) for irreversible effects. In the classical continuum-mechanics setting, state variables are transported by a flow map $\mathbf{x}(\mathbf{X}, t)$ through kinematics. For overdamped systems (neglecting inertia, $\mathcal{K} = 0$), the coupled LAP-MDP structure leads to a force-balance relation of the schematic form

$$\frac{\delta \mathcal{D}_{\text{mech}}}{\delta \mathbf{x}_t} = -\frac{\delta \mathcal{F}}{\delta \mathbf{x}}, \quad (14)$$

where \mathcal{F} is the Helmholtz free energy and $\mathcal{D}_{\text{mech}}$ is the mechanical dissipation potential. To place chemical kinetics on the same variational footing, Ref. (71) proposes carrying out the variation in Eq. 14 with respect to a reaction trajectory (or extent of reaction) $\mathbf{R}(t)$ (72, 73) and its time derivative. The reaction trajectory plays a role analogous to the flow map in mechanics, recording the net progress of the forward reactions up to time t and its time derivative can be interpreted as a reaction “velocity” (72).

This energetic variational formulation provides a unified template for chemo-mechanical systems: the mechanical and chemical subsystems share the same free-energy functional \mathcal{F} , but are associated with different dissipation mechanisms (and thus different rate laws) (71, 74). Technical details and illustrative examples are provided in the Supplementary Materials.

A three-state model by EnVarA

In this subsection, we first derive a thermodynamically consistent three-state model in the case that $V(t) = 0$. We consider a minimal single-head model on one periodic repeat unit on a thick filament. More detailed N -head formulations that incorporate cooperative effects can be built within the same framework by adopting the setting in (75). Following the classic framework of Huxley (8) and Duke (23), we assume that the binding sites on the thin filament are discrete and sufficiently far apart relative to the reach of a myosin head. Consequently, at any given time, each head can interact with at most one binding site. This allows us to define $x \in [-l, l]$ to be the relative displacement of a binding site on the thin filament with respect to the equilibrium (unstrained) position of the myosin head. l can be understood as the maximum possible extension of the cross-bridge tail (11). Since our primary goal is to illustrate the modeling framework rather than to perform a comprehensive physiological description, we intentionally neglect higher-level biological details such as lattice geometry, explicit S1/S2 microstructure and filament compliance beyond an effective internal coordinate, and cooperative interactions among neighboring heads (30).

Following T. L. Hill’s work (58), we assume the cross-bridge has three chemical states: state 1 (detached), state 2 (attached pre-stroke), and state 3 (attached post-stroke), defined in Eq. 6. For each $i \in \{1, 2, 3\}$, let $p_i(x, t)$ be the probability density of being in state i at coordinate x at time t . Thus p_i has units of $(\text{length})^{-1}$ and we impose the normalization $\sum_{i=1}^3 \int_{-l}^l p_i(x, t) dx = 1$. Let $G_i(x)$ denote the

effective free-energy landscape per head in state i , so that the mechanical force generated by the attached states at x is $F_i(x) = -\partial_x G_i(x)$ for $i = 2, 3$. A typical choice of $G_i(x)$ is given by Eq. 10. Let c_j ($j = 1, 2, 3$) denote the molecular line densities (number of molecules per unit length) of ATP, ADP, P_i in the local periodic micro-environment. We will use c_{ATP} , c_{ADP} , c_{P_i} interchangeably with (c_1, c_2, c_3) when it improves readability.

To model the chemo-mechanical cycle, we introduce three reaction trajectories (extents of reaction) $R_{12}(x, t)$, $R_{23}(x, t)$, and $R_{31}(x, t)$ associated with the Hill cycle defined in Eq. 7, respectively. Their time derivatives

$$r_{ab}(x, t) := \partial_t R_{ab}(x, t), \quad (ab) \in \{12, 23, 31\}, \quad (15)$$

are the (net) reaction rates.

For each state i , denote by $u_i(x, t)$ the drift velocity in the internal coordinate for heads in state i . For each chemical species j , denote by $v_j(x, t)$ the transport velocity of c_j . Due to the mass conservation, p_i and c_j satisfies the kinematics

$$\partial_t p_i + \partial_x(p_i u_i) = J_i, \quad \partial_t c_j + \partial_x(c_j v_j) = S_j \quad (16)$$

where the source terms are induced by the cycle rates r_{ab} :

$$J_1 = -r_{12} + r_{31}, \quad J_2 = r_{12} - r_{23}, \quad J_3 = r_{23} - r_{31}, \quad (17)$$

and the chemical production/consumption terms are

$$S_{\text{ATP}} = -r_{31}, \quad S_{\text{ADP}} = r_{31}, \quad S_{P_i} = r_{23}. \quad (18)$$

We define the total free energy on the unit cell as

$$\begin{aligned} \mathcal{F}[\mathbf{p}, \mathbf{c}] = & \int_{-l}^l \sum_{i=1}^3 \left(k_B T p_i \ln \frac{p_i}{p^{\text{ref}}} + p_i G_i(x) \right) dx \\ & + \int_{-l}^l \sum_{j=1}^3 \left(k_B T c_j \left(\ln \frac{c_j}{c^\circ} - 1 \right) + c_j \mu_j^\circ \right) dx, \end{aligned} \quad (19)$$

where $p^{\text{ref}} = 1/(2l)$ is a reference density, c° is the reference molecular line density, and μ_j° are standard chemical potentials. The associated chemical potentials are

$$\begin{aligned} \mu_i &:= \frac{\delta \mathcal{F}}{\delta p_i} = k_B T \ln \frac{p_i}{p^{\text{ref}}} + G_i(x), \\ \mu_{c_j} &:= \frac{\delta \mathcal{F}}{\delta c_j} = k_B T \ln \frac{c_j}{c^\circ} + \mu_j^\circ. \end{aligned} \quad (20)$$

To construct a thermodynamically consistent dynamics via EnVarA, we specify a dissipation rate

$$\Delta = \int_{-l}^l \left[\sum_{i=1}^3 \zeta_i p_i |u_i|^2 + \sum_{j=1}^3 \varepsilon_j c_j |v_j|^2 + \Delta_{\text{rxn}} \right] dx, \quad (21)$$

where, $\zeta_i > 0$ and $\varepsilon_j > 0$ are friction coefficients. A convenient choice of reaction dissipation that guarantees nonnegative entropy production is (71)

$$\Delta_{\text{rxn}} = \sum_{(ab) \in \{12, 23, 31\}} k_B T \dot{R}_{ab} \ln \left(1 + \frac{\dot{R}_{ab}}{r_{ab}^-(x, t)} \right), \quad (22)$$

where $r_{ab}^-(x, t) > 0$ denotes the backward reaction rate for the elementary step $a \rightarrow b$.

By the standard variational procedure, the mechanical force balance gives

$$\zeta_i p_i u_i = -p_i \partial_x \mu_i, \quad \varepsilon_j c_j v_j = -c_j \partial_x \mu_{c_j}. \quad (23)$$

Consequently,

$$\begin{aligned} \partial_t p_i &= \partial_x \left(\frac{k_B T}{\zeta_i} \partial_x p_i + \frac{1}{\zeta_i} p_i \partial_x G_i(x) \right) + J_i, \\ \partial_t c_j &= \partial_x \left(\frac{k_B T}{\varepsilon_j} \partial_x c_j \right) + S_j. \end{aligned} \quad (24)$$

For the reactions, introduce the local affinities

$$\begin{aligned} \mathcal{A}_{12} &:= \mu_2 - \mu_1, & \mathcal{A}_{23} &:= \mu_3 - \mu_2 + \mu_{c_{P_i}}, \\ \mathcal{A}_{31} &:= \mu_1 - \mu_3 + \mu_{c_{ADP}} - \mu_{c_{ATP}}. \end{aligned} \quad (25)$$

The dissipation Δ_{rxn} implies the generalized mass-action form

$$\dot{R}_{ab} = r_{ab}^-(x, t) \left(\exp(-\mathcal{A}_{ab}/(k_B T)) - 1 \right), \quad (26)$$

where $(ab) \in \{12, 23, 31\}$ with backward reaction rate

$$r_{12}^- = k_{12}^-(x) p_2, \quad r_{23}^- = k_{23}^-(x) c_{P_i} p_3, \quad r_{31}^- = k_{31}^-(x) c_{ADP} p_1.$$

Equivalently, Eq. 26 can be written in the classical law-of-mass-action form as forward-minus-backward fluxes,

$$\begin{aligned} \dot{R}_{12} &= \alpha_{12} p_1 - \alpha_{21} p_2, & \dot{R}_{23} &= \alpha_{23} p_2 - \alpha_{32} c_{P_i} p_3, \\ \dot{R}_{31} &= \alpha_{31} c_{ATP} p_3 - \alpha_{13} c_{ADP} p_1, \end{aligned} \quad (27)$$

where the ratios α_{ab}/α_{ba} are determined by the energetic landscapes and standard chemical potentials through Eq. 25, ensuring local detailed balance (Eq. 8).

Mechanical power output and efficiency

Now, we incorporate the shortening velocity $V(t)$ into the model. Since shortening velocity carries cross-bridges with a certain displacement into smaller values of displacement (11), this induces a transport term in the microscopic Fokker–Planck equation

$$\partial_t p_i - V \partial_x p_i = \partial_x \left(\frac{k_B T}{\zeta_i} \partial_x p_i + \frac{1}{\zeta_i} p_i \partial_x G_i(x) \right) + J_i, \quad (28)$$

For the free energy (Eq. 21), by a direct calculation, we have

$$\begin{aligned} \frac{d}{dt} \mathcal{F}(\mathbf{p}, \mathbf{c}) &= \int_{-l}^l \sum_{i=1}^3 \mu_i \partial_t p_i + \sum_{j=1}^3 \mu_{c_j} \partial_t c_j \, dx \\ &= -V(t) \int_{-l}^l \sum_{i=1}^3 p_i \partial_x \mu_i \, dx - \Delta_{\text{mech}} - \Delta_{\text{chem,tran}} - \Delta_{\text{rxn}}, \end{aligned} \quad (29)$$

Here the mechanical dissipation associated with drift/diffusion is $\Delta_{\text{mech}} := \int_{-l}^l \sum_{i=1}^3 \frac{p_i}{\zeta_i} |\partial_x \mu_i|^2 \, dx \geq 0$, the chemical transport dissipation is $\Delta_{\text{chem,trans}} := \int_{-l}^l \sum_{j=1}^3 \frac{c_j}{\varepsilon_j} |\partial_x \mu_{c_j}|^2 \, dx \geq 0$, and the reaction dissipation Δ_{rxn} is the same as Eq. 22.

Mechanical power output. The new transport term $-V \partial_x p_i$ induces an additional term in the right-hand side, which accounts for mechanical power transfer from the microscopic cross-bridge dynamics to the macroscopic sliding motion. We define

$$P_{\text{slide}} = V(t) \int_{-l}^l \sum_{i=1}^3 p_i \partial_x \mu_i \, dx = V(t) F_{cb}, \quad (30)$$

where

$$F_{cb}(t) := \sum_{i=1}^3 \int_{-l}^l p_i(x, t) \partial_x \mu_i \, dx = \sum_{i=1}^3 \int_{-l}^l p_i(x, t) \partial_x G_i \, dx, \quad (31)$$

is the cross-bridge generated force. For $\mu_i = k_B T \ln(p_i/p_{\text{ref}}) + G_i(x)$, the entropic contribution integrates to zero under periodic or non-flux boundary condition.

In many experimental settings, the sliding velocity $V(t)$ is prescribed (velocity clamp). $P_{\text{slide}}(t)$ should be interpreted as the instantaneous work rate done by (or against) the motor assembly to maintain the imposed motion. More generally, one can formulate a micro-macro model by integrating the macroscopic energy and dissipation (e.g., by including an external load and/or elastic elements (76).) with the microscopic energy-dissipation law (Eq. 29) and derive the macroscopic equation for $V(t)$.

Chemical power input. Chemical free energy is supplied through ATP hydrolysis. Since one completed Hill cycle consumes one ATP, the chemical input power is naturally expressed in terms of the cycle flux. The net ATP turnover rate can be defined as

$$J_{\text{ATP}}(t) = \int_{-l}^l \dot{R}_{31}(x, t) \, dx, \quad (32)$$

and the corresponding chemical free-energy input rate is

$$P_{\text{chem}}(t) = \int_{-l}^l \dot{R}_{31}(x, t) \Delta\mu(x, t) \, dx, \quad (33)$$

where $\Delta\mu = \mu_{c_1} - \mu_{c_2} - \mu_{c_3}$. Here, we assume a separation of timescales between the chemical cycle and the macroscopic mechanics: the internal cycle relaxes to its (quasi-)steady flux on a fast timescale, whereas the macroscopic sliding variable (and hence the mechanical power output) varies on a slower timescale. Consequently, for the purpose of computing power budgets we may treat the cycle flux as being instantaneously equilibrated with the current mechanical state, i.e.,

$$J_{12}(t) \approx J_{23}(t) \approx J_{31}(t) =: J_{\text{cyc}}(t),$$

up to transient and discretization effects.

Efficiency and power budget. We define the instantaneous mechanical efficiency as the ratio of useful mechanical power output to chemical free-energy input,

$$\eta(t) = \frac{P_{\text{mech}}(t)}{P_{\text{chem}}(t)} = \frac{F_{cb}(t) V(t)}{\int_{-l}^l \dot{R}_{31}(x, t) \Delta\mu(x, t) dx}. \quad (34)$$

FROM THE THREE STATE MODEL TO HUXLEY'S MODEL

In this section, we show how Huxley-type transport–reaction equations can be derived from the micro–macro formulation through coarse-graining.

We consider a chemostatted regime in which the nucleotide concentrations $c_{\text{ATP}}, c_{\text{ADP}}, c_{P_i}$ (equivalently, the chemical potentials $\mu_{\text{ATP}}, \mu_{\text{ADP}}, \mu_{P_i}$) are prescribed. A defining feature of living cells is that ATP and ADP are maintained at a nonequilibrium ratio (33), so that the chemical affinity

$$\Delta\mu = \mu_{\text{ATP}} - \mu_{\text{ADP}} - \mu_{P_i} \quad (35)$$

enters the kinetics through local detailed balance, biasing the ratios of forward and backward propensities along the cross-bridge cycle. In the three-state Hill cycle (7), the transition $2 \rightarrow 3$ corresponds to the mechanical power stroke coupled with the release of inorganic phosphate P_i , while the transition $3 \rightarrow 1$ is driven by ATP binding, which induces cross-bridge detachment and the release of ADP. With this convention, local detailed balance Eq. 8 directly yields the total affinity $\beta\Delta\mu$ around the directed cycle Eq. 9 which is the sole source of nonequilibrium bias in the kinetics. Under the chemostatted condition setting, the full dynamics is reduced to the Fokker–Planck type model for molecular motor (77). An important feature in our three-state formulation we keep ATP/ADP/ P_i explicitly and let their concentrations modulate the reaction rates. Thus $\Delta\mu$ does *not* appear as an additive tilt or modification of the mechanical free-energy landscape; rather, it biases the stochastic dynamics by reshaping the transition rates between chemical states.

From the three-state model, we can obtain the classical two-state model (77, 78) by grouping two attached states, and define

$$p_-(x, t) := p_1(x, t), \quad p_+(x, t) := p_2(x, t) + p_3(x, t).$$

To be more precise, let the drift–diffusion operators be

$$\mathcal{L}_i p := \partial_x \left(D_i \partial_x p + \frac{1}{\zeta_i} p \partial_x G_i(x) \right), \quad D_i := \frac{k_B T}{\zeta_i}.$$

Summing the equations for p_2 and p_3 yields the exact identity

$$\partial_t p_+ - V \partial_x p_+ = \mathcal{L}_2 p_2 + \mathcal{L}_3 p_3 + \alpha_{12}(x) p_1 - \alpha_{31}(x) p_3 \quad (36)$$

which is not closed in terms of p_+ unless an additional closure is introduced.

We adopt a fast equilibrium approximation as the closure condition. Specifically, we assume that transition between the attached states 2 and 3 is much faster than both the transport timescale and the overall ATP turnover. Under this separation of timescales, the (local) detailed-balance relation for the $2 \rightleftharpoons 3$ transition implies that

$$p_2 \approx \alpha(x) p_+, \quad p_3 \approx (1 - \alpha(x)) p_+, \quad (37)$$

where

$$\alpha(x) = \frac{1}{1 + \exp(\beta(G_2(x) - G_3(x) - \mu_{P_i}))}, \quad (38)$$

which is determined by the energy landscapes as well as the concentration of P_i . By further assume that $\zeta_2 = \zeta_3 = \zeta$, we have

$$\mathcal{L}_2 p_2 + \mathcal{L}_3 p_3 = \partial_x \left(D \partial_x p_+ + \frac{1}{\zeta} p_+ \partial_x G_+ \right), \quad (39)$$

where

$$\partial_x G_+ = \alpha(x) \partial_x G_2 + (1 - \alpha(x)) \partial_x G_3. \quad (40)$$

One can view G_+ as the *effective attached free-energy landscape*. Although the three-state model introduces chemical driving through concentration-dependent reaction rates, in the reduced description the same driving can be interpreted as reshaping the effective attached landscape G_+ through $\alpha(x)$.

Finally, (p_-, p_+) satisfy the closed two-state coupled-diffusion system

$$\begin{aligned} \partial_t p_- - V \partial_x p_- &= \partial_x \left(D_1 \partial_x p_- + \frac{1}{\zeta_1} p_- \partial_x G_1 \right) - f(x) p_- + g(x) p_+, \\ \partial_t p_+ - V \partial_x p_+ &= \partial_x \left(D \partial_x p_+ + \frac{1}{\zeta} p_+ \partial_x G_+ \right) + f(x) p_- - g(x) p_+, \end{aligned} \quad (41)$$

which is the classical two-state Fokker–Planck type model for molecular motors (45, 77–79). Here, the effective transition rates are

$$f(x) := \alpha_{12}(x), \quad g(x) = \alpha_{31}(x) c_{\text{ATP}} (1 - \alpha(x)), \quad (42)$$

A direct calculation shows that

$$\frac{f(x)}{g(x)} = \frac{\alpha_{12}(1 + \exp(-\beta(G_2 - G_3 - \mu_{P_i})))}{\alpha_{31} c_{\text{ATP}}} \quad (43)$$

The system can further reduce to Huxley model (Eq. 3) by taking the limit of $D \rightarrow 0$ (77) and define $n(x, t) = p_+(x, t)$.

Compared with the original Huxley formulation, the present derivation provides an explicit, thermodynamically consistent characterization of how the attachment/detachment kinetics depend on both mechanical effects (through G_2, G_3 , and hence the x -dependence) and chemical driving (through $\Delta\mu$ via local detailed balance). Moreover, it clarifies how the nonequilibrium drive is inherited in the reduced description: $\Delta\mu$ influences the effective attached dynamics through $\alpha(x)$ (and thus the effective landscape G_+), while simultaneously biasing the effective reaction kinetics through Eq. 42.

NUMERICS: FROM HUXLEY TO A. V. HILL

In this section, we demonstrate that the reduced Huxley type two-state model reproduces a Hill-type force–velocity (F – V) relation. For a given shortening velocity V , the steady state of the reduced model $n(x)$ satisfies

$$-V \partial_x n(x) = f(x) (1 - n(x)) - g(x) n(x), \quad x \in [-l, l]. \quad (44)$$

We impose the boundary condition $n(l) = 0$ when $V(t) > 0$, the ODE (Eq. 44) has a unique solution. The macroscopic cross-bridge force is computed by integrating the mean microscopic tension:

$$F_{\text{cb}}(V) = \int_{-l}^l n(x; V) \partial_x G_+(x) dx, \quad (45)$$

where $G_+(x)$ is the effective attached free energy induced by the fast $2 \leftrightarrow 3$ equilibration, defined in Eq. 40. Although Eq. 44 can be solved analytically, the resulting expression involves nested integrals; instead, we solve it numerically using an upwind discretization. We discretize the interval $[-l, l]$ into N uniform subintervals with grid points $x_i = -l + i\Delta x$. We compute $n_i \approx n(x_i)$ from

$$-V \frac{n^{i+1} - n^i}{\Delta x} = f(x) - (f(x) + g(x))n^i \quad (46)$$

with the boundary condition $n^N = 0$. We take $l = 50$ (nm) and $N = 10000$ in all numerical results below.

The model parameters involved in the reduced model are $G_i(x)$, concentrations of ATP , ADP and P_i , and the reaction rates $\alpha_{12}(x)$ and $\alpha_{31}(x)$. Our goal here is qualitative. We adopt parameter values and functional forms motivated by classical cross-bridge and molecular-motor literature, but we do not attempt a systematic calibration or optimization. A data-driven parameter inference procedure, for example, fitting measured F–V curves together with ATPase rates or duty ratios, is left for future work.

We take $G_1(x) = 0$ define

$$\begin{aligned} G_2(x) &= -\Delta G_{\text{bind}} + \frac{\kappa}{2} q(x)^2, \\ G_3(x) &= -\Delta G_{\text{bind}} - \Delta G_{\text{stroke}} + \frac{\kappa}{2} q(x+d)^2 \end{aligned} \quad (47)$$

where $q(x) = x_0 \tanh(x/x_0)$ with $x_0 = 10$, $\kappa = 2\text{pN/nm}$, $\Delta G_{\text{bind}} = 4k_B T$, $G_{\text{stroke}} = 12k_B T$, and $d = 8\text{nm}$. In the small-displacement regime, $q(x) \approx x$, so $G_2(x)$ and $G_3(x)$ reduce to the quadratic (Hookean) landscapes used by Duke Eq. 10. This choice reflects the difference between continuous model and MD simulations. In a continuum Fokker–Planck/Huxley-type description, the displacement x is a continuous state variable and the evolution equation can advect probability mass toward the edges of the truncated x -domain. With a purely quadratic spring, the steady states may exhibit artificial accumulation near the imposed boundaries and the computed force can become sensitive to the chosen cutoff and

boundary conditions. We therefore introduce the saturating map $q(x) = x_0 \tanh(x/x_0)$ to regularize the large- $|x|$ behavior and mitigate boundary-driven artifacts, while preserving the Hookean limit in the working range. In contrast, in MD-based simulations extreme displacements are unlikely to be sampled over accessible times because geometric constraints and finite reach effectively confine the motion; as a result, the dynamics typically does not “run into” such artificial boundaries, and an explicit continuum-level cutoff is less critical.

For the transition rate α_{12} and α_{31} , we choose simple analytic forms that reflect standard qualitative assumptions: (i) attachment is localized near a preferred binding strain (a “reach” region), and (ii) detachment is accelerated in the negative-strain “drag” region to avoid excessive compressive loading. Specifically, we take

$$\alpha_{12}(x) = 20 \exp\left(-\frac{1}{2} \left(\frac{x-2}{3}\right)^2\right), \quad (48)$$

and

$$\alpha_{31}(x) = 10 + \frac{20}{1+\exp(x+2)}. \quad (49)$$

We emphasize that these profiles are neither unique nor intended to be optimal, and they are not necessarily chosen to reflect detailed biological considerations. Nevertheless, our numerical simulations show that this choice is sufficient to reproduce a Hill-type force–velocity curve. We take $\mu_{P_i} = 0$ in the numerical simulations.

Fig. 1 shows the simulation result with $c_{\text{ATP}} = 3c_0$, where c_0 is a reference concentration used for nondimensionalization. In our formulation, concentration factors are absorbed into the rate constants, so only the dimensionless ratio c_{ATP}/c_0 enters the effective kinetics. Fig. 1(a) shows the normalized tension–velocity relation F/F_0 as a function of the shortening velocity V . As V increases from the isometric condition ($V = 0$), the predicted tension decreases monotonically and exhibits the characteristic concave shape of a Hill-type force–velocity (F–V) curve: a rapid drop at small velocities followed by a gradual approach toward near-zero tension at large velocities. The chemo-mechanical dependence of the attachment and detachment rates $f(x)$ and $g(x)$ captures the basic shape of Hill’s force–velocity curve. With a representative (non-calibrated) parameter choice, the predicted curve is in reasonable agreement with classical benchmarks (6, 8, 30). Fig. 1(b) shows steady-state attached distributions $n(x)$ at several velocities. At $V = 0$, $n(x)$ is sharply localized near the force-generating region, indicating a high duty fraction and a narrowly distributed cross-bridge extension. With increasing V , the distribution broadens and its peak height decreases substantially, reflecting a reduced fraction of attached cross-bridges and a shift toward configurations that contribute less force. Consequently, both the duty ratio and the mean force-bearing strain decrease with V , leading to a smaller average tension and giving rise to the Hill-type F–V relation in the left panel.

We further examine the dependence of the force–velocity relation on ATP availability by varying the chemostatted ATP

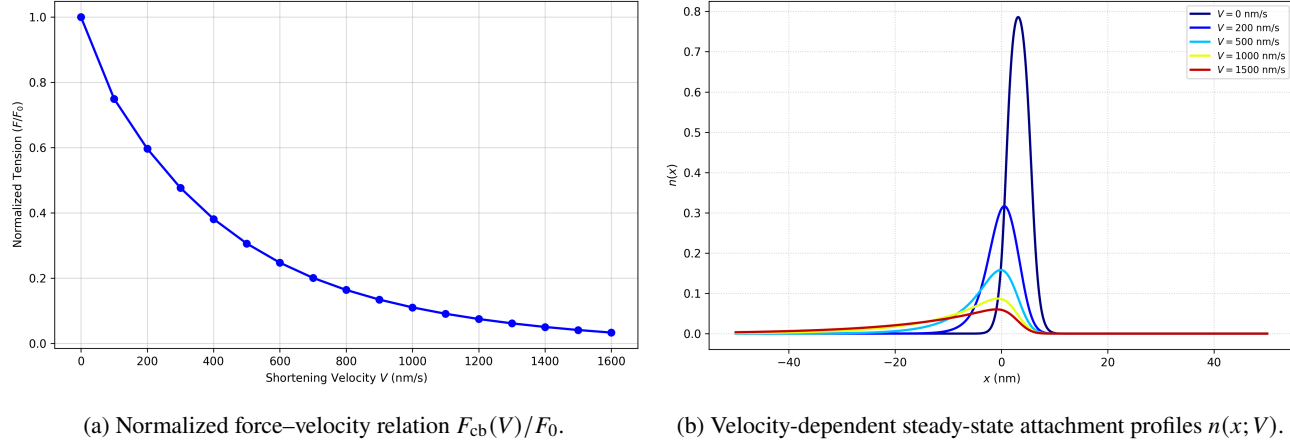


Figure 1: From the reduced Huxley-type model to a Hill-type F–V curve. (a): normalized cross-bridge force $F_{cb}(V)/F_0$, where $F_{cb}(V)$ is computed by Eq. 45 using $n(x; V)$ and $F_0 := F_{cb}(0)$. (b): steady-state solutions $n(x; V)$ of Eq. 44 for representative shortening velocities.

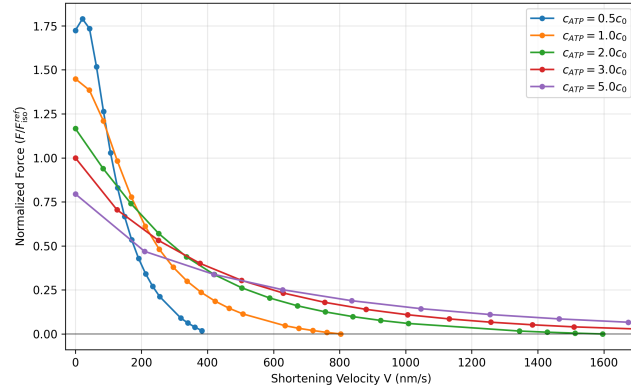


Figure 2: The effect of ATP concentration on the force-velocity relation. Forces are normalized by the isometric tension at the reference concentration ($c_{ATP} = 3c_0$).

level c_{ATP}/c_0 . Figure 2 shows force-velocity ($F - V$) relations across a range of ATP concentrations (c_{ATP}), normalized by the isometric force at a reference physiological concentration ($3c_0$). We observe a distinct crossover behavior driven by the competition between attachment probability and detachment kinetics. At vanishing velocities ($V \rightarrow 0$), lower ATP concentrations paradoxically yield higher isometric tensions. This arises because the detachment rate $g(x)$ is proportional to c_{ATP} ; thus, scarce ATP prolongs the attached lifetime of cross-bridges, increasing the steady-state duty ratio. However, this static advantage is rapidly lost during shortening. At low c_{ATP} , the slow detachment becomes rate-limiting, causing cross-bridges to be dragged into the compressive region ($x < 0$) before they can dissociate. These over-stretched heads generate a significant viscous drag that opposes motion. In contrast, saturating ATP levels ensure rapid detachment, suppressing this drag effect and allowing the system to sustain

positive force even at high shortening velocities.

CONCLUSION

In this work we developed a thermodynamically consistent chemo-mechanical framework that bridges classical cross-bridge kinetics and Hill-type muscle mechanics. Starting from a three-state Hill cycle, we derived a three-state Fokker-Planck-jump model in which the chemical driving enters through local detailed balance, biasing the jump rates between mechanical states. Under chemostatted conditions, and with a fast-equilibration closure for the attached substates, the microscopic dynamics reduces to a closed two-state Fokker-Planck-type model for molecular motors (42, 77, 78). In the further singular limit where the microscopic diffusion in the attached state vanishes, this description recovers a Huxley-type transport-reaction equation (8). Numerical simulations show the steady states of the reduced system reproduce a Hill-like force-velocity relation. Taken together, these results provide a transparent pathway *from a three-state FP-jump description to Huxley-type kinetics and finally to Hill-type macroscopic behavior*. A key contribution of the present formulation is the *thermodynamic closure* inherited from the energetic variational structure. While the current study is intended as a proof of concept and does not yet exploit the full potential of this structure in parameter calibration or quantitative prediction, the variational framework provides a principled definition of macroscopic force and efficiency that are not explicit in the original two-state or phenomenological Huxley formulations. This built-in accounting of energy and dissipation also clarifies how chemical nonequilibrium driving is transmitted to the reduced kinetics through the effective rates and force generation.

Several directions are natural next steps. First, a data-driven *parameter inference* is needed to quantitatively connect

the model to experiments, for example by jointly fitting force-velocity curves with ATPase rates, duty ratios, and transient relaxation data. Second, extending the numerics beyond the chemostatted setting to simulate the *full model*, including spatiotemporal ATP/ADP/ P_i dynamics, will enable the study of ATP-limited regimes and supply constraints. Third, the energetic formulation makes it possible to investigate *efficiency and heat generation* in a unified manner (60); incorporating explicit heat production (or temperature dependence) would allow direct comparison with classical measurements of heat and work in muscle. Finally, it will be important to couple the present microscopic description to *macro-scale mechanics* (80), for instance through force balance with external load and filament compliance, to establish a consistent micro-macro closure that links cross-bridge kinetics, force generation, and tissue-level mechanical response.

DECLARATION OF GENERATIVE AI

During the preparation of this work, the author(s) used ChatGPT in order to improve Language. After using this tool/service, the author(s) reviewed and edited the content as needed and take(s) full responsibility for the content of the published article.

AUTHOR CONTRIBUTIONS

Y.W.: Conceptualization, Methodology, Investigation, Writing – Original Draft, Writing – Review & Editing. C.L.: Conceptualization, Methodology, Writing – Review & Editing.

ACKNOWLEDGMENTS

Y. W. was partially supported by NSF DMS-2410740. C. L. was partially supported by NSF DMS-2410742 and DMS-2216926. The authors thank Prof. Thomas C. Irving for fruitful discussions on the biological background.

REFERENCES

1. Fung, Y.-c., 2013. Biomechanics: mechanical properties of living tissues. Springer Science & Business Media.
2. Qian, H., 2008. Viscoelasticity of living materials: Mechanics and chemistry of muscle as an active macromolecular system. *Molecular & Cellular Biomechanics* 5:107.
3. Hirokawa, N., 1998. Kinesin and dynein superfamily proteins and the mechanism of organelle transport. *Science* 279:519–526.
4. Prodanovic, M., Y. Wang, S. M. Mijailovich, and T. Irving, 2023. Using multiscale simulations as a tool to interpret equatorial X-ray fiber diffraction patterns from skeletal muscle. *International Journal of Molecular Sciences* 24:8474.
5. Powers, J. D., S. A. Malignen, M. Regnier, and T. L. Daniel, 2021. The sliding filament theory since Andrew Huxley: multiscale and multidisciplinary muscle research. *Annual Review of Biophysics* 50:373–400.
6. Hill, A. V., 1938. The heat of shortening and the dynamic constants of muscle. *Proceedings of the Royal Society of London. Series B-Biological Sciences* 126:136–195.
7. Baker, J. E., 2024. Mixed-scale versus multiscale models of muscle contraction. *Biophysical Journal* 123:3646–3647.
8. Huxley, A. F., 1957. Muscle structure and theories of contraction. *Prog. Biophys. Biophys. Chem* 7:255–318.
9. HUXLEY, H., and J. HANSON, 1954. Changes in the cross-striations of muscle during contraction and stretch and their structural interpretation. *Nature* 173:973–976.
10. Huxley, A. F., and R. Niedergerke, 1954. Structural changes in muscle during contraction: interference microscopy of living muscle fibres. *Nature* 173:971.
11. Williams, W., 2011. Huxley's model of muscle contraction with compliance. *Journal of elasticity* 105:365–380.
12. Seow, C. Y., 2013. Hill's equation of muscle performance and its hidden insight on molecular mechanisms. *The Journal of general physiology* 142:561–573.
13. Huxley, A. F., and R. M. Simmons, 1971. Proposed mechanism of force generation in striated muscle. *Nature* 233:533–538.
14. Peskin, C. S., 1975. Mathematical aspects of heart physiology. *Courant Inst. Math.*
15. Lynn, R., and E. W. Taylor, 1971. Mechanism of adenosine triphosphate hydrolysis by actomyosin. *Biochemistry* 10:4617–4624.
16. Williams, W. O., 1984. On the Lacker-Peskin model for muscular contraction. *Mathematical biosciences* 70:203–216.
17. Lacker, H., and C. Peskin, 1986. A mathematical method for the unique determination of cross-bridge properties from steady-state mechanical and energetic experiments on macroscopic muscle, AMS, volume 16, 121–153.
18. Pate, E., and R. Cooke, 1989. A model of crossbridge action: the effects of ATP, ADP and P i. *Journal of Muscle Research & Cell Motility* 10:181–196.
19. Greene, L. E., and E. Eisenberg, 1980. Cooperative binding of myosin subfragment-1 to the actin-tropomyosin complex. *Proceedings of the National Academy of Sciences* 77:2616–2620.

20. Zahalak, G. I., 1981. A distribution-moment approximation for kinetic theories of muscular contraction. *Math. Biosci.* 55:89–114.
21. Smith, D., and M. Geeves, 1995. Strain-dependent cross-bridge cycle for muscle. *Biophys. J.* 69:524–537.
22. Smith, D., and M. Geeves, 1995. Strain-dependent cross-bridge cycle for muscle. II. Steady-state behavior. *Biophys. J.* 69:538–552.
23. Duke, T., 1999. Molecular model of muscle contraction. *Proceedings of the National Academy of Sciences* 96:2770–2775.
24. Cordova, N. J., B. Ermentrout, and G. F. Oster, 1992. Dynamics of single-motor molecules: the thermal ratchet model. *Proceedings of the National Academy of Sciences* 89:339–343.
25. Piazzesi, G., and V. Lombardi, 1995. A cross-bridge model that is able to explain mechanical and energetic properties of shortening muscle. *Biophys. J.* 68:1966.
26. Chin, L., P. Yue, J. J. Feng, and C. Y. Seow, 2006. Mathematical simulation of muscle cross-bridge cycle and force-velocity relationship. *Biophys J* 91:3653–3663.
27. Smith, D., M. A. Geeves, J. Sleep, and S. M. Mijailovich, 2008. Towards a unified theory of muscle contraction. I: foundations. *Annals of biomedical engineering* 36:1624–1640.
28. Smith, D. A., and S. M. Mijailovich, 2008. Toward a unified theory of muscle contraction. II: predictions with the mean-field approximation. *Annals of biomedical engineering* 36:1353.
29. Marcucci, L., and L. Truskinovsky, 2010. Muscle contraction: A mechanical perspective. *The European Physical Journal E* 32:411–418.
30. Mijailovich, S. M., O. Kayser-Herold, B. Stojanovic, D. Nedic, T. C. Irving, and M. A. Geeves, 2016. Three-dimensional stochastic model of actin–myosin binding in the sarcomere lattice. *The Journal of general physiology* 148:459–488.
31. Caruel, M., and L. Truskinovsky, 2018. Physics of muscle contraction. *Reports on Progress in Physics* 81:036602.
32. Vilfan, A., E. Frey, and F. Schwabl, 1999. Force-velocity relations of a two-state crossbridge model for molecular motors. *EPL (Europhysics Letters)* 45:283.
33. Qian, H., 2005. Cycle kinetics, steady state thermodynamics and motors—a paradigm for living matter physics. *Journal of Physics: Condensed Matter* 17:S3783.
34. Williams, W. O., 1990. A purely mechanical theory of muscular contraction. *Mathematical biosciences* 100:249–278.
35. Peskin, C. S., G. M. Odell, and G. F. Oster, 1993. Cellular motions and thermal fluctuations: the Brownian ratchet. *Biophys J* 65:316–324.
36. Hill, T. L., 1974. Theoretical formalism for the sliding filament model of contraction of striated muscle Part I. *Progress in biophysics and molecular biology* 28:267–340.
37. Hill, T. L., E. Eisenberg, Y. Chen, and R. J. Podolsky, 1975. Some self-consistent two-state sliding filament models of muscle contraction. *Biophysical journal* 15:335–372.
38. Hill, T. L., 1976. Theoretical formalism for the sliding filament model of contraction of striated muscle part II. *Progress in biophysics and molecular biology* 29:105–159.
39. Eisenberg, E., and T. L. Hill, 1985. Muscle contraction and free energy transduction in biological systems. *Science* 227:999–1006.
40. Astumian, R. D., and M. Bier, 1996. Mechanochemical coupling of the motion of molecular motors to ATP hydrolysis. *Biophysical journal* 70:637–653.
41. Qian, H., 1997. A simple theory of motor protein kinetics and energetics. *Biophys. Chem.* 67:263–267.
42. Parmeggiani, A., F. Jülicher, A. Ajdari, and J. Prost, 1999. Energy transduction of isothermal ratchets: Generic aspects and specific examples close to and far from equilibrium. *Physical Review E* 60:2127.
43. Bustamante, C., D. Keller, and G. Oster, 2001. The physics of molecular motors. *Acc Chem Res* 34:412–420.
44. Wang, H., and G. Oster, 2002. Ratchets, power strokes, and molecular motors. *Applied Physics A* 75:315–323.
45. Chipot, M., D. Kinderlehrer, and M. Kowalczyk, 2003. A variational principle for molecular motors. *Meccanica* 38:505–518.
46. Kolomeisky, A. B., and M. E. Fisher, 2007. Molecular motors: a theorist’s perspective. *Annu. Rev. Phys. Chem.* 58:675–695.
47. Mogilner, A., T. C. Elston, H. Wang, and G. Oster, 2002. Molecular motors: theory. In *Computational cell biology*, Springer, 320–353.
48. Wagoner, J. A., and K. A. Dill, 2016. Molecular motors: Power strokes outperform Brownian ratchets. *The Journal of Physical Chemistry B* 120:6327–6336.

49. Hwang, W., and M. Karplus, 2019. Structural basis for power stroke vs. Brownian ratchet mechanisms of motor proteins. *Proceedings of the National Academy of Sciences* 116:19777–19785.

50. Peskin, C. S., and G. Oster, 1995. Coordinated hydrolysis explains the mechanical behavior of kinesin. *Biophysical journal* 68:202S.

51. Visscher, K., M. J. Schnitzer, and S. M. Block, 1999. Single kinesin molecules studied with a molecular force clamp. *Nature* 400:184–189.

52. Vale, R. D., and R. A. Milligan, 2000. The way things move: looking under the hood of molecular motor proteins. *Science* 288:88–95.

53. Atzberger, P. J., and C. S. Peskin, 2006. A Brownian dynamics model of kinesin in three dimensions incorporating the force-extension profile of the coiled-coil cargo tether. *Bulletin of mathematical biology* 68:131.

54. Astumian, R. D., 2015. Huxley’s model for muscle contraction revisited: the importance of microscopic reversibility. *Polymer Mechanochemistry* 285–316.

55. Barclay, C., 2011. Energetics of contraction. *Comprehensive physiology* 5:961–995.

56. Woledge, R. C., N. A. Curtin, and E. Homsher, 1985. Energetic aspects of muscle contraction. *Monographs of the physiological society* 41:1–357.

57. Kimmig, F., D. Chapelle, and P. Moireau, 2019. Thermodynamic properties of muscle contraction models and associated discrete-time principles. *Advanced Modeling and Simulation in Engineering Sciences* 6:6.

58. Hill, T. L., 2005. Free energy transduction and biochemical cycle kinetics. Courier Corporation.

59. Giga, M.-H., A. Kirshtein, and C. Liu, 2016. Variational Modeling And Complex Fluids. In A. Novotny, and Y. Giga, editors, *Handbook of Mathematical Analysis in Mechanics of Viscous Fluids*, Springer.

60. Wang, Y., and C. Liu, 2022. Some recent advances in energetic variational approaches. *Entropy* 24:721.

61. Doi, M., 2011. Onsager’s variational principle in soft matter. *Journal of Physics: Condensed Matter* 23:284118.

62. Wang, H., T. Qian, and X. Xu, 2021. Onsager’s variational principle in active soft matter. *Soft Matter* 17:3634–3653.

63. Wang, Q., 2020. Generalized Onsager principle and its applications. In *Frontiers and progress of current soft matter research*, Springer, 101–132.

64. Grmela, M., and H. C. Öttinger, 1997. Dynamics and thermodynamics of complex fluids. I. Development of a general formalism. *Physical Review E* 56:6620.

65. Öttinger, H. C., and M. Grmela, 1997. Dynamics and thermodynamics of complex fluids. II. Illustrations of a general formalism. *Physical Review E* 56:6633.

66. Rayleigh, L., 1873. Some General Theorems Relating to Vibrations. *Proceedings of the London Mathematical Society* 4:357–368.

67. Onsager, L., 1931. Reciprocal relations in irreversible processes. I. *Phys. Rev.* 37:405.

68. Onsager, L., 1931. Reciprocal relations in irreversible processes. II. *Phys Rev* 38:2265.

69. Erickson, J. L., 1992. Introduction to the Thermodynamics of Solids.

70. Liu, C., and J.-E. Sulzbach, 2020. The Brinkman-Fourier System with Ideal Gas Equilibrium. *arXiv preprint arXiv:2007.07304*.

71. Wang, Y., C. Liu, P. Liu, and B. Eisenberg, 2020. Field theory of reaction-diffusion: Mass action with an energetic variational approach. *arXiv preprint arXiv:2001.10149*.

72. Kondepudi, D., and I. Prigogine, 2014. *Modern thermodynamics: from heat engines to dissipative structures*. John Wiley & Sons.

73. Oster, G. F., and A. S. Perelson, 1974. Chemical reaction dynamics. *Arch. Ration. Mech. Anal.* 55:230–274.

74. Wang, Y., 2025. Energetic Variational Modeling of Active Nematics: Coupling the Toner–Tu Model with ATP Hydrolysis. *Entropy* 27:801.

75. Mouri, K., and T. Shimokawa, 2008. The Fokker-Planck approach for the cooperative molecular motor model with finite number of motors. *Biosystems* 93:58–67.

76. Zahalak, G. I., 1990. Modeling muscle mechanics (and energetics). In *Multiple muscle systems*, Springer, 1–23.

77. Qian, H., 2000. The mathematical theory of molecular motor movement and chemomechanical energy transduction. *J. Math. Chem.* 27:219–234.

78. Jülicher, F., and J. Prost, 1998. Molecular motors: From individual to collective behavior. *Progress of Theoretical Physics Supplement* 130:9–16.

79. Jülicher, F., A. Ajdari, and J. Prost, 1997. Modeling molecular motors. *Reviews of Modern Physics* 69:1269.

80. Borja da Rocha, H., and L. Truskinovsky, 2019. Functionality of disorder in muscle mechanics. *Physical Review Letters* 122:088103.